J Geod (2014) 88:1131–1143
DOI 10.1007/s00190-014-0748-2

ORIGINAL ARTICLE

Using DORIS measurements for modeling the vertical total electron content of the Earth's ionosphere

Denise Dettmering · Marco Limberger · Michael Schmidt

Received: 10 April 2014 / Accepted: 7 July 2014 / Published online: 26 July 2014

Abstract The Doppler orbitography and radiopositioning integrated by satellite (DORIS) system was originally developed for precise orbit determination of low Earth orbiting (LEO) satellites. Beyond that, it is highly qualified for modeling the distribution of electrons within the Earth's ionosphere. It measures with two frequencies in L-band with a relative frequency ratio close to 5. Since the terrestrial ground beacons are distributed quite homogeneously and several LEOs are equipped with modern receivers, a good applicability for global vertical total electron content (VTEC) modeling can be expected. This paper investigates the capability of DORIS dual-frequency phase observations for deriving VTEC and the contribution of these data to global VTEC modeling. The DORIS preprocessing is performed similar to commonly used global navigation satellite systems (GNSS) preprocessing. However, the absolute DORIS VTEC level is taken from global ionospheric maps (GIM) provided by the International GNSS Service (IGS) as the DORIS data contain no absolute information. DORIS-derived VTEC values show good consistency with IGS GIMs with a RMS between 2 and 3 total electron content units (TECU) depending on solar activity which can be reduced to less than 2 TECU when using only observations with elevation angles higher than 50°. The combination of DORIS VTEC with data from other space-geodetic measurement techniques improves the accuracy of global VTEC models significantly. If DORIS VTEC data is used to update IGS GIMs, an improvement of up to 12 % can be achieved. The accuracy directly beneath the DORIS satellites' ground-tracks ranges between 1.5 and 3.5 TECU assuming a precision of 2.5 TECU for altimeter-derived VTEC values which have been used for validation purposes.

Keywords DORIS · Ionosphere · VTEC

D. Dettmering (✉) · M. Limberger · M. Schmidt
Deutsches Geodätisches Forschungsinstitut (DGFI),
Alfons-Goppel-Strasse 11, 80539 München, Germany
e-mail: dettmering@dgfi.badw.de

1 Introduction

Information on ionospheric parameters such as the vertical total electron content (VTEC) is essential for manifold applications in various fields, e.g. navigation, telecommunication, and geodesy. In addition to climatological models such as the International Reference Ionosphere (IRI) (Bilitza and Reinisch 2008) data-driven models gain more and more influence as they can provide higher accuracies even in time periods with anomalous events such as solar storms. Nowadays, most of the data-driven ionosphere models are based on observations from global navigation satellite systems (GNSS), especially from the global positioning system (GPS). The most prominent examples are the global ionosphere maps (GIM) from the International GNSS Service (IGS) (Dow et al. 2009; Hernández-Pajares et al. 2009). However, GNSS is not the only geodetic observation technique able to provide information on the distribution of the free electrons in the Earth's ionosphere. As the latter is a dispersive medium for microwaves one can use nearly any observation system providing measurements on two or more frequencies for ionosphere modeling.

In the last years, several investigations on the combination of multiple observation techniques for ionosphere modeling and especially for VTEC modeling have been published: Todorova et al. (2007) showed a combination of GNSS with satellite radar altimetry (RA) which was enlarged by Alizadeh et al. (2011) to radio occultation measurements (RO) from space-based GPS. Moreover, observations from

very long baseline interferometry (VLBI) can be incorporated (Dettmering et al. 2011b). In addition to these measurement methods there exists another space-geodetic observation technique which can contribute to ionospheric research: Doppler orbitography and radiopositioning integrated by satellite (DORIS) (Willis et al. 2007).

First ionospheric applications with DORIS data were published more than 20 years ago by Foucher and Ciavaldini (1991) and Fleury et al. (1991). More recently, Li and Parrot (2007) used DORIS TEC data to study ionospheric response to seismic events and Bernhardt and Siefring (2010) analyzed ionospheric scintillations based on DORIS signals measured by the CITRIS instrument on board of STPSat1. Since that time, the DORIS system improved significantly (Auriol and Tourain 2010). The ground station network (also called ground beacon network) has been expanded, new satellite missions are equipped with DORIS receivers, the receiver technique has been improved, and new data formats are established. After first tests with DORIS ionospheric information extracted from satellite altimetry products (Dettmering et al. 2011a), 2013 used the new DORIS phase measurements collected on board of Jason-2 (Mercier et al. 2010) for ionosphere modeling in combination with other space-based observation techniques. In the study on hand, these investigations are extended to all available DORIS missions equipped with the improved version of the DORIS receiver and the complete DORIS ground beacon network for global modeling.

The purpose of this paper is to demonstrate the capacity of DORIS for the estimation of ionospheric VTEC, to check its consistency with other observation techniques, and to investigate its impact on ionosphere model results and accuracies. The paper is separated in three main parts: Sect. 2 describes the DORIS system and the observation used in this study. Afterwards, the DORIS preprocessing is handled specifying the derivation of VTEC data from the original measurements (Sect. 3). This is followed by a section introducing the ionosphere modeling itself including the model results and validations (Sect. 4). The paper terminates with conclusions and an outlook to further work.

2 DORIS system and data

DORIS is a French satellite tracking system developed for precise orbit determination (POD) of low Earth orbiting satellites (LEO). It is based on the principle of the Doppler effect and consists of satellite-based antenna-receiver systems on board of several LEOs and a transmitting terrestrial beacon network sending two signals L_1 and L_2 on the frequencies $f_1 = 2,036.25$ MHz and $f_2 = 401.25$ MHz.

Both signals are effected by the ionosphere. However, the impact on L_1 is less than on L_2 due to the higher frequency. Compared to the GPS frequencies (1,575.42 and 1,227.60 MHz), DORIS L_1 is less influenced than GPS L_1 and DORIS L_2 shows larger impact than GPS L_2. Even more important is the separation of the two frequencies which is for DORIS significantly larger than for GPS. The ratio of the two frequencies is close to 5, in comparison to 1.3 for GPS. This leads to lower influence of the ionospheric signal by measurement errors and thus to higher system sensitivity regarding ionospheric information. However, due to the low second frequency, the second order ionospheric effects may no longer be neglected (cf. Sect. 3.1).

DORIS measurements are collected on-board and delivered to the ground generally once per revolution. Hence, unlike GPS, no real-time processing of DORIS data on ground is possible. However, this also permits the absence of internet connection at beacon level.

2.1 DORIS station distribution and satellite missions

Since the terrestrial stations only need a power supply and no further communication technique (in contrast to GNSS station which require internet access to transmit the observation data) it is possible to operate DORIS ground beacons on isolated islands. Consequently, the global distribution of DORIS stations is almost uniform. In 2014, the system consists of nearly 60 stations whose locations are visualized in Fig. 1.

In the beginning of 2014, five satellite missions are equipped with DORIS receivers and more reveivers are scheduled for several new missions. To be more specific, the first satellite mission equipped with DORIS was SPOT2 in the early 90th followed by TOPEX/Poseidon in 1992. Most of the current and past radar altimeter missions use DORIS (together with other systems) for POD, among them Jason-1 and Envisat. Today, DORIS is installed on Jason-2, Cryosat-2, HY-2A, SARAL, and SPOT5. Moreover, it will fly on future missions such as Jason-3 and Sentinel-3.

2.2 DORIS data and formats used in the present study

Within the last years, the DORIS system improved significantly. For instance, new receiver types were developed. The most recent instrument generation (the third one) is called DGXX being a payload of Jason-2, Cryosat-2, HY-2A, and SARAL. In contrast to older instruments, these new receivers directly provide continuous dual-frequency phase measurements (Mercier et al. 2010) in RINEX DORIS 3.0 format (Lourme 2010) from seven parallel channels. Moreover, pseudo-range code observations are available. However, the latter are rarely usable for most applications due to their large measurement noise of about 1 km (Mercier et al. 2010). The sampling interval is fixed to 10 s with one inter-

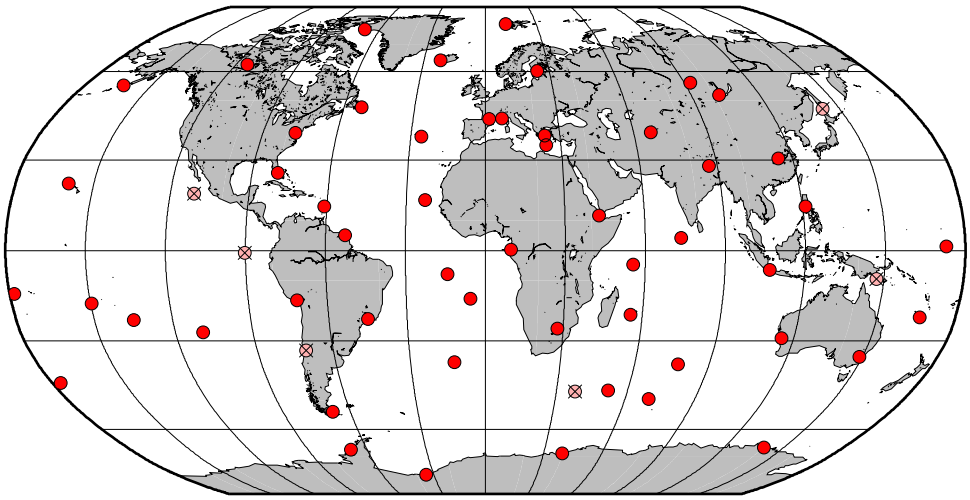

Fig. 1 DORIS ground beacon network (end of 2013). Active stations (between mid September and mid of November) are marked in *red* (#53) and inactive stations or stations with only very few observations are indicated by *light red and crosses* (#6)

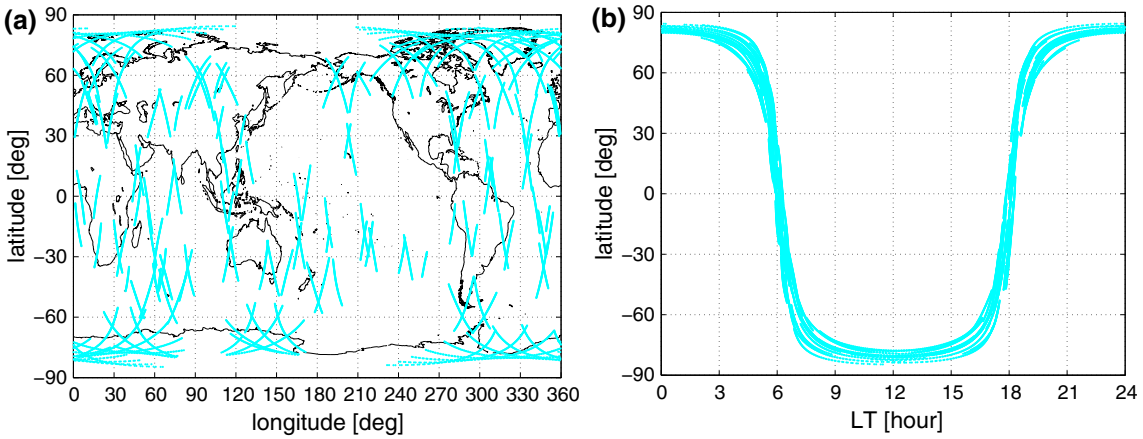

Fig. 2 DORIS observations from the SARAL mission for 24 hs (DOY 258 / Sept 15, 2013). The *left plot* (**a**) shows the distribution within a geographical coordinate system and the same distribution with local time (LT) is illustrated on the *right-hand side* (**b**)

mediate measurement shifted by 3 s. In the present study, data from all epochs are used with time intervals of 3 and 7 s, respectively. The data are freely available at the data centers of the International DORIS Service (IDS), for more details see Willis et al. (2010).

In order to investigate the performance of DORIS for ionosphere modeling a global data set of all DGXX equipped missions (Jason-2, Cryosat-2, HY-2A, and SARAL) is used. As the most recent mission (SARAL) was launched in February 2013, this study will only use data from late 2013, namely 2 months from September, 15th until November, 15th (day of year (DOY) 258-319). During that time period, the number of active DORIS beacons is 53. However, not all of them are usable for each mission. The number of stations with valid observations ranges between 46 and 53 for a single mission.

Although the geographical distribution of DORIS ground beacons is global and quite homogenous (cf. Fig. 1), the measurement distribution strongly depends on the orbits of the missions which are used. Within 24 h all four LEOs achieve an almost global data coverage within a geographical coordinate system (Fig. 2a for SARAL). However, due to the Earth rotation, the coverage in local time (LT) is limited as can be seen in Fig. 2b. Thus, global VTEC modeling is rarely possible with only one mission. Only by a combination of several DORIS missions or a combination with other observation techniques high resolution models (in time and space) can be computed. The combined utilization of four DORIS missions seems promising. However, even with these four missions, for some time periods the data distribution is not homogenous. This strongly depends on the interrelation of the local times of ascending nodes (LTAN) of the single missions. Some DORIS missions (such as SARAL flying on a sun-synchronous orbit) have a fixed LTAN, for other missions LTAN changes with different rates (as given in Table 1 and illustrated for the time period of investigation in Fig. 3) leading to day-to-day variations in the data coverage.

Table 1 Theoretical rate of right ascension of the ascending node Ω (due to J2) and empirical change of local time of ascending node ($LTAN$) for the DORIS DGXX missions

Mission	$\dot{\Omega}$ [°/days]	$\dot{LTAN}$ [h/10 days]
Jason-2	−2.0743	−2.0
HY-2A	0.9834	0.0
SARAL	0.9862	0.0
Cryosat-2	0.2390	−0.2

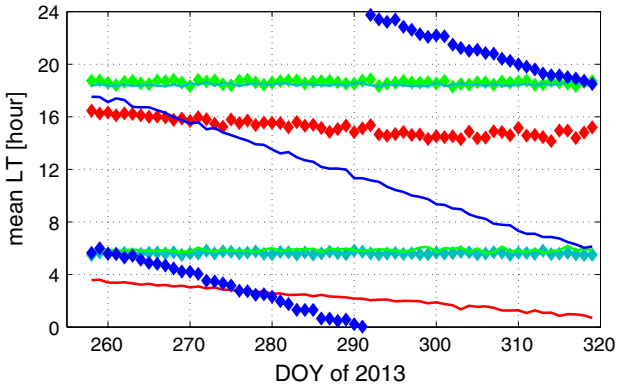

Fig. 3 Mean local time (LT) per day for ascending (*diamonds*) and descending (*lines*) passes of Jason-2 (*blue*), Cryosat-2 (*red*), HY-2A (*green*), and SARAL (*cyan*)

3 DORIS data preprocessing

In order to derive VTEC observations from the original DORIS phase measurements several preprocessing steps have to be conducted. Some computations are similar to the standard GNSS preprocessing since the input measurements are comparable. However, some differences remain which are discussed in the following in more detail.

The first preprocessing step is the derivation of slant total electron content (STEC) from DORIS phase measurements. Therefore, each observation is linked to the corresponding station and satellite positions. For defining the observation time the DORIS receiver clock offsets given within the RINEX observation files are taken into account in order to refer all observations to international atomic time (TAI). This is primarily important for SARAL as this mission—at least in the early data sets—exhibits a clock bias of more than 200 s which is by two orders of magnitude larger than for the other three missions. The orbit information are interpolated from final orbits in SP3 format (Hilla 2010) using Lagrange interpolation (Schueler 1998). Afterwards, the ionospheric observables are computed. The new generation of DORIS DGXX receivers provide dual-frequency synchronous phase measurements as well as code pseudo-ranges. Since the latter are disrupted by a strong noise level, the computation of the ionospheric delay is solely based on carrier phase data. The observation equation referring to a carrier-phase observable in range units on a specific frequency i is given by

$$\lambda_i \Phi_i = D_i + \delta^s - \delta_b + \lambda_i N_i + \delta_i^{\text{ion}} + \delta_e + \epsilon_i \tag{1}$$

including the wavelength λ_i related to the carrier frequency and the measured phase Φ_i on the left-hand side. The right-hand side includes a geometry term denoted as D_i that depends on the positions of the receiver and transmitter antennas, clock biases δ_b, δ^s of the ground-based DORIS beacon b and the orbiting receiver s, the unknown number N_i of cycles between satellite and receiver, the ionospheric delay δ_i^{ion}, and further influences by non-dispersive effects δ_e (e.g., troposphere, ocean loading, tides, relativistic effects). The observation error is indicated by ϵ_i.

Phase variations due to the phase wind-up effect (PWU) are neglected here. The PWU is caused by continuous rotation of the satellite to align its solar panels towards the sun and depends on the relative orientation between transmitter- and receiver antenna as well as the line of sight direction. Following Mercier and Cerri (2010), PWU for Jason-2 yields a maximum of 30 cm (which corresponds to a complete flip of the spacecraft) but it is much smaller for almost all passes and negligible for Cryosat-2. Within this study, the PWU is neglected for all missions but it has to be kept in mind that it can reach the decimeter level depending on the satellite mission and the satellite's attitude.

Based on Eq. (1), the geometry-free, or ionospheric linear combination for dual-frequency measurements yields

$$\begin{aligned}\lambda_1 \Phi_1 - \lambda_2 \Phi_2 \\ = D_1 - D_2 + \delta_1^{\text{ion}} - \delta_2^{\text{ion}} + \lambda_1 N_1 - \lambda_2 N_2 + \epsilon_1 - \epsilon_2\end{aligned} \tag{2}$$

where the non-dispersive effects are naturally canceled. Equation (2) can be reformulated by

$$\lambda_1 \Phi_1 - \lambda_2 \Phi_2 = \Delta D + \frac{1}{k} \delta_1^{\text{ion}} + N + \epsilon \tag{3}$$

to obtain the ionospheric delay with respect to the first frequency. For this purpose, a frequency dependent factor $k = f_2^2 / \left(f_2^2 - f_1^2\right)$ implying both frequencies f_1 and f_2 is introduced. Here, the geometry correction is substituted by ΔD, the combined ambiguity term is denoted as $N = \lambda_1 N_1 - \lambda_2 N_2$ and the measurement errors on both frequencies are merged to ϵ. The ionospheric delay related to the first carrier frequency in range units follows from

$$\delta_1^{\text{ion}} = k \left(\lambda_1 \Phi_1 - \lambda_2 \Phi_2 - \Delta D\right) + N + \epsilon \tag{4}$$

with N and ϵ having still the same definition but different content because of factor k. Neglecting higher order ionospheric effects, the computation of the ionospheric impact in terms of STEC in total electron content units (TECU) with 1 TECU= 10^{16}el/m^2 is a straightforward task and yields

$$\begin{aligned}\mathrm{STEC} &= -\frac{f_1^2}{40.3}\delta_1^{\mathrm{ion}}10^{-16} \\ &= -\frac{f_1^2}{40.3}\left(k\left(\lambda_1\Phi_1-\lambda_2\Phi_2-\Delta D\right)+N+\epsilon\right)10^{-16}.\end{aligned} \tag{5}$$

The geometry correction ΔD can be easily computed from the known differences of the antenna phase centers for the two frequencies (cf. Sect. 3.2), whereas N and ϵ remain as unknowns in the data. In the following step, a pass detection is performed to separate continuous data arcs during the observation phase between a specific receiver and a DORIS beacon. The approach is simple and considers mainly the detection of larger jumps in the ionospheric range delay $((\delta_1^{\mathrm{ion}}|_{t-1} - \delta_1^{\mathrm{ion}}|_t) > T)$ between consecutive epochs in comparison with a previously defined threshold $T = 0.2$ m. Furthermore, each pass is screened by a 3-sigma outlier test, i.e. each measurement of a specific pass is proven to be below the threshold of 3σ and, if this limit is exceeded, the observation is removed. This procedure is performed iteratively until no observation above the 3σ level is left. As a last step, passes that do not contain a defined minimum number of 40 observations are omitted. This reduces the data by between 14 % (Jason-2) and 27 % (Cryosat-2). The final products resulting from the preprocessing routine are pass-wise biased (or ambiguous) STEC observations with up to 250 measurements per pass.

3.1 Higher order ionospheric effects

In Eq. (5) higher order ionospheric effects are neglected. This is acceptable for high frequencies but may invoke errors for decreasing frequencies. Following Petit and Luzum (2010) the second order effect reaches about 0.1 % of the first order effect for GPS L_1 frequency and about 1 % for frequencies around 150 MHz. Thus, for DORIS L_2 the influence of higher order terms might be significant. It depends—in addition to the signal frequency—on the magnetic field strength and direction in relation to the signal path. Thus, for the computation, some information or model of the magnetic field is necessary.

Since all higher order ionospheric effects have been neglected in the present study, they may impact the results and are part of the differences and accuracies given in the validation part of this paper. Following Mercier and Cerri (2010) the influence on DORIS L_2 can reach up to 60 cm (approximately 3 TECU).

3.2 Geometry correction

The two DORIS signals travel on different paths, especially due to the differences in the location of the antenna phase center for both frequencies (in space as well as on ground). Consequently, the geometric distance differs for both signals. Not accounting for this effect will reach a maximum of 65 cm range error for the 400 MHz signal of Jason-2. (Mercier and Cerri 2010).

Table 2 Phase center locations for the two phase centers 1 and 2 taken from Cerri and Ferrage (2014) and corresponding nadir difference d^s for the missions used in this investigation

Mission	$x_1/y_1/z_1$ [m] $x_2/y_2/z_2$ [m]	d^s [m]
Jason-2	1.194 / −0.598 / 1.022	0.1640
	1.194 / −0.598 / 0.858	
HY-2A	0.850 / −0.750 / 1.306	0.1620
	0.850 / −0.750 / 1.144	
SARAL	0.805 / −0.304 / −1.129	0.1580
	0.647 / −0.304 / −1.129	
Cryosat-2	1.848 / −0.200 / −0.751	0.1538
	1.832 / −0.200 / −0.598	

Table 2 lists the phase center definitions for the four satellites used in this investigation and the geometry correction d^s derived from these values. It should be noted that the satellites' coordinate systems differ for the missions and the given locations are not directly comparable. An antenna dependent ground station correction d_b has to be added to d^s in order to compute the overall geometry correction which can be converted to a range difference $\Delta D = D_1 - D_2$ (cf. Eqs. (2)–(5)) using the satellites elevation angle e according to

$$D_1 - D_2 = \Delta D \approx -d \cdot \sin e \qquad \text{with} \qquad d = d^s + d_b. \tag{6}$$

This formula is only an approximation neglecting the curvature of the satellite orbit. Following IDS (2012) the value $d_b = 0.487$ m for the Starec antennae and $d_b = 0.175$ m for the former Alcatel antennae are applied.

3.3 Absolute STEC level

Fixing the absolute level of DORIS STEC data [i.e. estimating the ambiguity term N in Eq. (5)] is much more demanding than for GNSS due to the fact that the DORIS pseudo-range measurements are strongly impacted by noise and cannot be used for carrier-smoothing or code-leveling. Alternatively, external information must be utilized to determine the absolute STEC level. In the present study, data from the IGS GIMs are taken for fulfilling this task. For this purpose, for each DORIS observation the corresponding ionospheric pierce point (IPP) is computed and used to extract IGS VTEC which is then scaled to the appropriate DORIS satellites orbit height (more information in Sect. 3.5) and mapped to STEC using a simple mapping function which is described in more detail in Sect. 3.4. From the difference between the DORIS

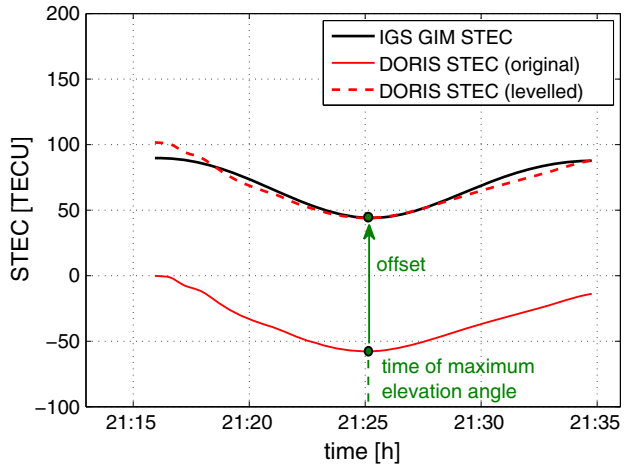

Fig. 4 DORIS STEC for one Jason-2 descending pass of station Kourou (KRWB) on DOY 258/2013 before (*red bold line*) and after (*dashed red line*) levelling to IGS GIM (*black line*). The maximum elevation angle of this pass yields nearly 80°

STEC and the GIM STEC one offset per satellite pass is estimated. This is computed by building the STEC difference (DORIS minus IGS GIM) of the observation with the maximum elevation per pass as illustrated in Fig. 4.

Using this method ensures a minimum mapping error in the GIM data. The whole pass is discarded in case the maximum elevation does not exceed 20° or the standard deviation σ_o of the estimated offset (computed from the differences in each point of the pass) exceeds a threshold of 5 TECU. This reduces the number of valid passes by about 3.5 %. Table 3 summarizes some statistics of the estimated offsets for 24 h. The offsets mainly depend on the absolute STEC (which is highly correlated with local time of observation) as the first observation of each pass equals zero due to the DORIS measurement principle providing only relative phase measurements. This effect is illustrated in Fig. 5 for Jason-2.

The reader should notice that the leveling is necessary to allow for an accurate mapping of the DORIS STEC to VTEC since otherwise the elevation-independent phase ambiguity will impact the mapping accuracy. Later, the absolute DORIS VTEC level may be changed again within the ionosphere modeling itself (Sect. 4) by estimating constant offsets for each pass, each mission, or for the whole DORIS system.

Furthermore, it shall be emphasized that using this level fixing method no differential code biases (DCB) like for GNSS have to be estimated as these values are already part of the individual pass offsets.

3.4 Mapping STEC to VTEC

For the conversion of STEC to VTEC a simple single-layer ionosphere model is used, based on the assumption that all free electrons are concentrated in one thin shell with

Table 3 Statistics of estimated offsets for all passes for DOY 258

Mission	Offset range [TECU]	Mean σ_o [TECU]	Number of passes
Jason-2	−144.9 … 2.7	1.29	199
HY-2A	−119.6 … 3.7	1.34	191
SARAL	−164.3 … −2.5	1.50	169
Cryosat-2	−187.1 … 8.5	1.60	158

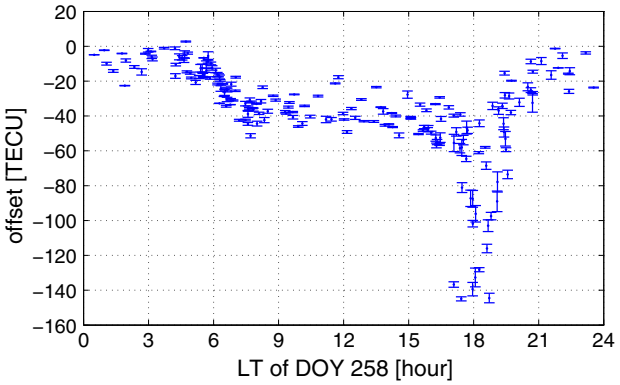

Fig. 5 Estimated STEC offsets for each Jason-2 pass for DOY 258. The offsets are plotted in dependence to the mean local time (LT) per pass. The *error bars* shows the standard deviations σ_o

constant height H above the Earth's surface. To be more specific, the modified single-layer mapping function $m_f(z)$ introduced many years ago by the Center for Orbit Determination in Europe (CODE) (Hugentobler et al. 2002) is applied with $H = 506.7\,\text{km}$, $\alpha = 0.9782$, and an Earth radius $R = 6371\,\text{km}$. This mapping function

$$m_f(z) = \frac{1}{\cos z'} \quad \text{with} \quad \sin z' = \frac{R}{R+H}\sin(\alpha \cdot z) \tag{7}$$

only depends on the zenith angle z of the observation. The observed STEC has to be divided by m_f to derive the VTEC in the IPP defined by the intersection of the signal path with the thin shell.

3.5 Handling different orbit heights (VTEC scaling)

Due to the basic measurement geometry the DORIS VTEC values only comprises the electron content below the satellite's orbit which is different for each mission and—as DORIS flies on LEOs—far below GNSS orbit heights. To combine VTEC measurements derived by different DORIS missions a conversion to one consistent upper height is necessary. This becomes even more important if a combination with GNSS derived VTEC is foreseen. In the present study, all VTEC values are scaled to GPS orbit height of about 20,200 km in order to be able to compare the results to IGS products. Of course, these scaling process adds further errors to the data.

Table 4 Scaling factors used to convert DORIS VTEC from LEO orbit height to GPS orbit height (kindly provided by R.Scharroo)

Mission	Approx. orbit height (km)	Scaling factor
Jason-2	1,350	1/0.925
HY-2A	970	1/0.880
SARAL	800	1/0.856
Cryosat-2	720	1/0.744

Table 5 VTEC differences to global VTEC models (GPS orbit height); mean $\pm\sigma$ in [TECU] for the 51 stations active on DOY 258

Mission	IGS GIM	NIC09	IRI07
Jason-2	-0.11 ± 1.74	-6.80 ± 4.04	-11.03 ± 7.62
HY-2A	-0.10 ± 1.84	-6.27 ± 4.02	-11.55 ± 7.86
SARAL	-0.16 ± 1.94	-6.62 ± 4.19	-10.45 ± 8.36
Cryosat-2	-0.07 ± 2.02	-6.80 ± 5.08	-10.39 ± 10.48

There are several possibilities to conduct the VTEC scaling, e.g. the use of models or of relative fractions derived from models. In this study, fixed factors are used for each orbit height to scale the DORIS VTEC to GPS orbit height. Scharroo and Smith (2010) showed that only small differences exist between the use of constant factors and factors derived from IRI fractions (as proposed by Iijilma et al. 1999). These factors—commonly used by the altimeter community to correct single-frequency altimeter measurements—are given in Table 4.

3.6 Comparison of DORIS VTEC to global models

Before using the DORIS VTEC data for ionosphere modeling a validation of this data set is performed. This is conducted by comparing the data to external global VTEC models. Three different models are used for this investigation: (1) IRI07 (Bilitza and Reinisch 2008), (2) NIC09 model (Scharroo and Smith (2010), and (3) IGS GIM (Hernández-Pajares et al. 2009). The first two models are climatological using only sparse input data to account for actual solar activity. In contrast, IGS GIMs are based on actual GNSS measurements. However, it should be kept in mind, that this model had already been used to fix the unknown phase ambiguities of the DORIS STEC measurements. All comparisons are conducted in GPS orbit height, i.e. after mapping the DORIS STEC to VTEC (Sect. 3.4) the values are scaled to GPS orbit height of about 20,200 km as described in Sect. 3.5.

Before the whole time period of two months is analyzed, a closer look at the first day (DOY 258) is done in order to show dependencies on elevation and local measurement time. Table 5 summarizes the results of the comparison of DORIS VTEC with the three external global models for DOY 258.

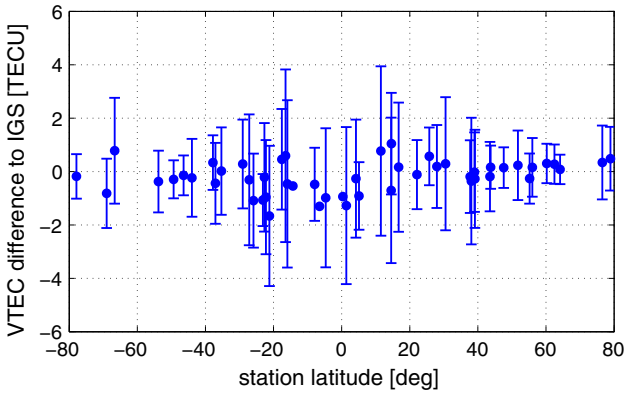

Fig. 6 Mean differences of Jason-2 DORIS VTEC with respect to IGS GIM (DOY 258). The mean differences per station are plotted together with their standard deviations. Observations with elevations smaller 10° are discarded

It gives the average difference for each mission and the corresponding standard deviation value. Naturally, the mean difference with respect to the IGS model is about zero as this model has been used for the absolute STEC leveling (cf. Sect. 3.3). However, looking on the differences per station one can identify mean differences up to 4 TECU (for Cryosat-2, not shown). For 97 % of the stations the mean differences remain smaller than 2 TECU, for 84 % smaller than 1 TECU, respectively. For Jason-2 these mean differences are illustrated in Fig. 6. These remaining offsets provide an impression on the accuracy of the performed STEC leveling (cf. Sect. 3.3). The mean differences with respect to the two climatological models are larger. They are clearly dominated by model errors and do not reflect the DORIS accuracies. Probably, both models overestimate the global mean VTEC due to the extraordinary low current solar cycle.

The standard deviation values in Table 5 shows only small inter-mission differences and are about two times larger for IRI07 than for NIC09. IGS GIM achieves the best consistency (σ of about 2 TECU) which is twice as small as for NIC09. In addition, the standard deviations of the VTEC differences depends on the station latitude (most probably due to the different absolute VTEC levels) as can be seen in Fig. 6 for Jason-2 and IGS.

Since the IGS model clearly outperforms the two other models, only differences to IGS GIM will be analyzed in the following in more detail. The differences show a clear dependence on the measurement's elevation angles as illustrated in Fig. 7 for all four missions. By using only observations with elevation angles larger than 50° one can reduce the RMS of the differences to values below 1 TECU. Figure 7 also indicates a correlation with local measurement time represented by ascending or descending orbit passes: nighttime or early morning measurements (ascending passes

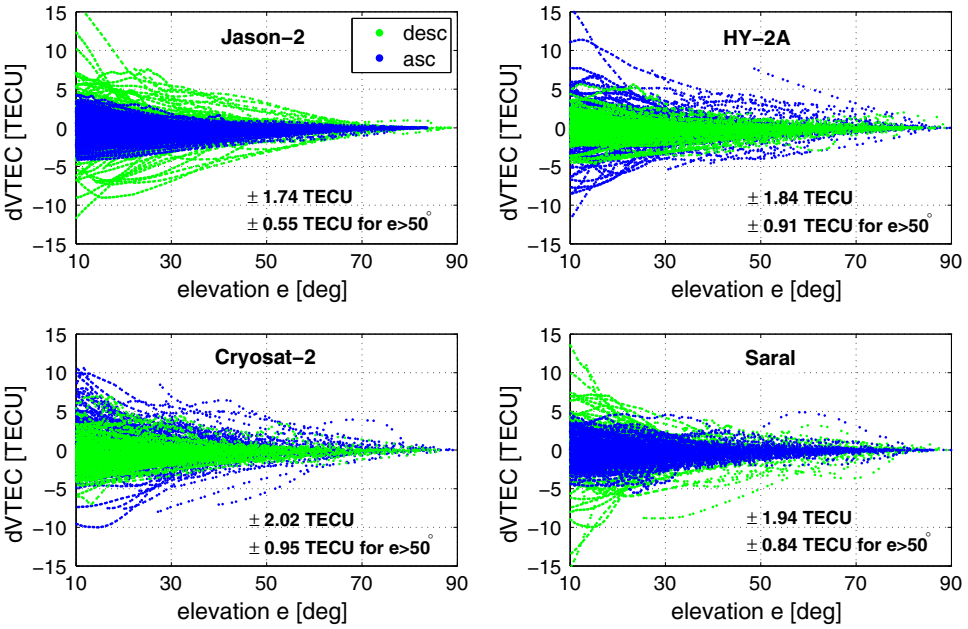

Fig. 7 VTEC differences in GPS orbit height: DORIS minus IGS GIM for four different missions depending on measurement elevation angle e in [TECU] for DOY 258. Measurements from ascending passes are plotted in *blue*, those from descending passes in *green*

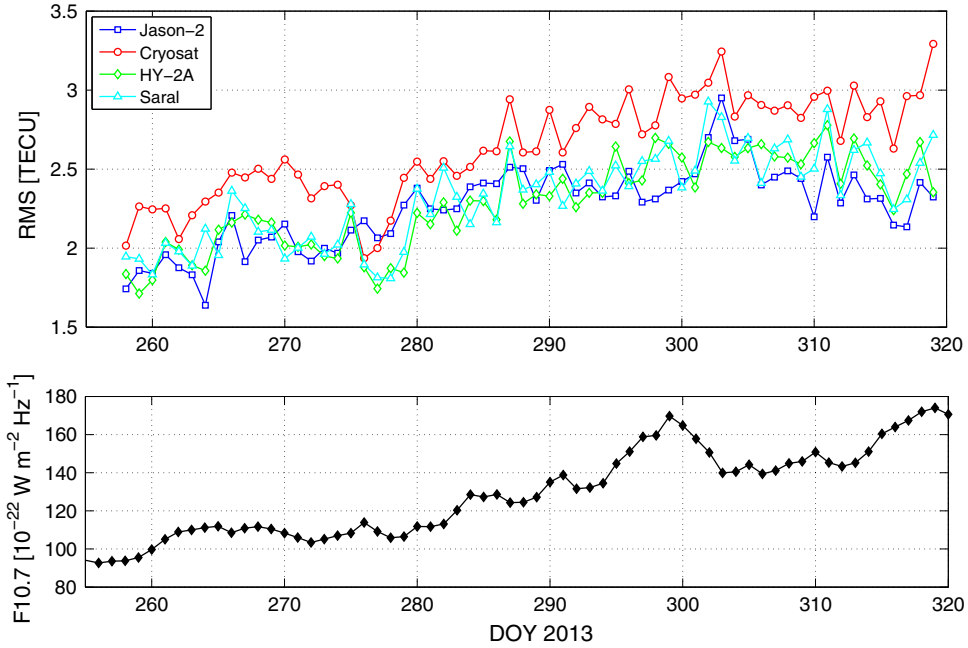

Fig. 8 Daily RMS values of VTEC differences with respect to IGS GIM in [TECU] with elevation cutoff of 10° (*top plot*) and the solar radio flux F10.7 for the same time period (*bottom plot*)

for Jason-2 and SARAL; descending passes for HY-2A and Cryosat-2) show less differences to VTEC model values than daytime passes. Naturally, not all of these differences are due to DORIS uncertainties. Also mapping function effects, scaling errors, and GIM modeling effects are visible here.

In addition to dependencies on elevation and local time, there is a clear connection of DORIS VTEC differences to the solar activity. When looking at the RMS values of all stations for a longer time period of 2 months one can see a clear correlation with global solar radio flux F10.7 (NOAA 2014) which indicates the radio emission from the Sun at a wavelength of 10.7 cm. This is illustrated in Fig. 8 for all four DORIS missions under investigation. The nearly linear increase in solar activity between DOY250 and DOY300 (bottom plot) is also visible in the differences between DORIS observations and IGS model which increase from about 2 TECU up to between 2.5 and 3 TECU RMS. Probably, both data sets—DORIS VTEC observations as well as IGS models—show decreased accuracies with increasing solar activity.

An inter-mission comparison between the four DORIS missions in the top plot of Fig. 8 shows that Cryosat-2 performes slightly worse than the other missions. This is prob-

Table 6 Mean VTEC differences to IGS GIM (RMS in [TECU]) during the whole time period of investigation (Sept. 15–Nov. 15, 2013) for the four DORIS missions using different elevation cutoff angles

Mission	$e > 10°$	$e > 50°$	Mean improvement
Jason-2	2.48	1.83	0.65
HY-2A	2.31	1.88	0.42
SARAL	2.32	1.32	1.00
Cryosat-2	2.57	2.07	0.51

ably due to the fact that Cryosat's ascending passes are all measured between 14 and 16 o'clock LT which is the time of highest solar radiation. In contrast, the other three missions show local measurement times of 6 and 18 o'clock (SARAL and HY-2A), and variable LT (Jason-2), respectively (cf. Fig. 3).

Using a higher elevation cutoff angle will decrease the RMS values significantly. Especially for SARAL the consistency to IGS GIM is very good since the mean RMS is below 1.5 TECU when only comparing observations with high elevations (more than 50°). But also the other missions improved significantly and show differences about or less than 2 TECU RMS (cf. Table 6). The dependency with solar flux remains visible when using other elevation cutoffs (not shown).

4 Global VTEC models based on DORIS measurements

In this section the preprocessed DORIS VTEC data are used to estimate model parameters describing the spatial and temporal properties of the Earth's ionosphere. In the first subsection the theoretical model approach is described briefly before selected results are presented in Sects. 4.2 and 4.3 using two different background models: NIC09 (climatological) and IGS GIM (data driven). Since IRI07 perfomed worst in the VTEC comparisons (cf. Sect. 3.6) it is not used for further studies.

4.1 Model approach

The ionospheric model approach used in this study has already been introduced in detail in Schmidt et al. (2011). Here, only the basic facts are recapitulated and described. In the first step we decompose VTEC depending on geographical latitude ϕ and longitude λ as well as time t according to

$$\begin{aligned} &\mathrm{VTEC}(\phi, \lambda, t) \\ &\quad = \mathrm{VTEC}_{\mathrm{back}}(\phi, \lambda, t) + \Delta\mathrm{VTEC}(\phi, \lambda, t) \end{aligned} \tag{8}$$

into a given background model $\mathrm{VTEC}_{\mathrm{back}}$ (e.g. NIC09) and an unknown correction part ΔVTEC. The latter is represented by the series expansion

$$\begin{aligned} &\Delta\mathrm{VTEC}(\phi, \lambda, t) \\ &\quad = \sum_{k_1=0}^{K_1-1} \sum_{k_2=0}^{K_2-1} \sum_{k_3=0}^{K_3-1} d_{k_1,k_2,k_3}\, B_{k_1}^{J_\phi}(\phi) T_{k_2}^{J_\lambda}(\lambda)\, B_{k_3}^{J_t}(t) \end{aligned} \tag{9}$$

in terms of three-dimensional basis functions defined as the tensor product of three one-dimensional basis functions. To be more specific, a set of one-dimensional trigonometric B-spline functions T depending on longitude λ and two sets of one-dimensional end-point interpolating polynomial B-spline functions B depending on latitude ϕ and time t are combined. The B-spline levels J_λ, J_ϕ, and J_t define the number of functions for each variable according to $K_1 = 2^{J_\phi} + 2$, $K_2 = 3 \cdot 2^{J_\lambda} + 2$ and $K_3 = 2^{J_t} + 2$. The numerical values for the three levels are defined by the averaged sampling intervals of the input data sets; see Schmidt et al. (2011).

The altogether $K = K_1 \cdot K_2 \cdot K_3$ unknown series coefficients d_{k_1,k_2,k_3} of Eq. (9) shall be estimated within an adjustment process such as least squares estimation. Special attention has to be drawn to the polar regions where additional constraints have to be considered (Schumaker and Traas 1991). Furthermore, due to possible data gaps the normal equation system might be singular or at least ill-conditioned. In order to overcome these problems prior information for the expectation vector and the covariance matrix of the coefficients d_{k_1,k_2,k_3} is introduced. Moreover, besides the series coefficients the model also contains unknown constant offsets for each observation group with respect to the background model. In this way, systematic biases between the different observation groups are accounted for. More details are given by Dettmering et al. (2011a).

Since the parameter estimation shall be based on a variety of different input data types (such as DORIS and GNSS), the weighting of the observation groups and the prior information has to be handled appropriate. For this purpose, a variance component estimation (VCE) following Koch and Kusche (2002) is used.

4.2 VTEC model with NIC09 as background

Due to the inadequate spatial-temporal distribution of the DORIS VTEC observations a reliable computation of global DORIS-only models is not possible for most of the days—even if four DORIS missions are available. However, DORIS can be used in combination with other observation techniques, such as terrestrial GNSS, RO, or RA.

In order to check the impact of DORIS to combined VTEC models three different model solutions for DOY 258/2013 were computed based on different input data sets: GPS only, GPS+RO, and GPS+RO+DORIS. For all solutions NIC09 was used as background model and a model resolution of $J_\lambda = J_\phi = J_t = 3$ (L333) was applied, i.e. 2600 model coefficients were estimated, together with about 120 addi-

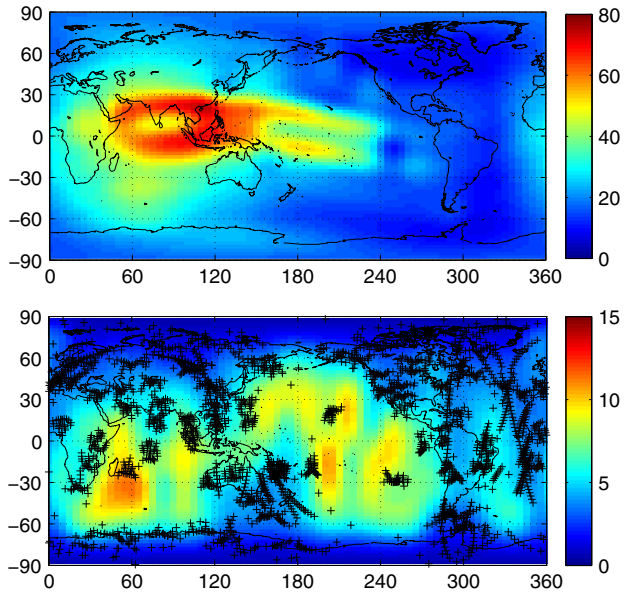

Fig. 9 Model result for DOY 258, 8 UTC based on NIC09 background model and observations from terrestrial GPS, RO, and four DORIS missions. The *top plot* shows the estimated VTEC. The formal errors are illustrated in the *bottom plot* together with the input data distribution (black crosses represent the IPP). All information in [TECU]

tional daily constants for differential code biases for GPS and systematic offsets for each DORIS mission. The amount of coefficients representing the geographical distribution (260) corresponds to the number of the unknowns of a spherical harmonic expansion up to degree 15 (256) as it is used by CODE. This yields a spatial model resolution of about 20° and a temporal resolution of about 2.7 h.

Data of 87 GPS stations (part of IGS network) were used together with RO observations of the FORMOSAT-3/COSMIC mission (Fong et al. 2009). Altimeter measurements were not incorporated in these models since these data are saved for validation purposes.

The model result for 8 UTC of DOY 258 (based on all three observation techniques GPS, RO, and DORIS) is illustrated in Fig. 9. In the bottom plot, one can clearly see that the model precision is decreased significantly in areas with sparse or no observations. In order to quantify the contribution of DORIS, comparisons of all three model results with IGS GIM and RA measurements of Jason-2 were performed. Table 7 presents the consistency of these models which are based on different input data types with IGS GIM and RA measurements. As the input data for all models is only sparse and the background model NIC09 used for filling the data gaps is climatological, the quality of all three models is not as good as those of other data-driven global models. Nevertheless, it is clearly visible that including DORIS VTEC into the model improves the internal model precision σ_{vtec} (improvement of about 45 % with respect to GPS only model)

Table 7 Statistics of different VTEC models (L333) in comparison with IGS GIM and RA (Jason-2) for DOY258

Input data	Mean σ_{vtec}	RMS wrt IGS GIM	RMS wrt RA
GPS	9.2	5.8	6.28
GPS, RO	8.2	5.4	6.16
GPS, RO, DORIS	5.0	4.5	5.44

All numbers in TECU

as well as the consistency with respect to IGS GIMs (about 22 %) and RA measurements (about 13 %).

4.3 VTEC model with IGS GIM as background

Since an insufficient overall data distribution is not able to overcome a poor background model, NIC09 is replaced by IGS GIM in this section. As additional input data solely DORIS VTEC data are used. Since these observations are all located in a small area around the satellites' ground-tracks most parts of the globe are still represented by the background model. However, this measurement geometry will be perfectly qualified for improving the IGS GIM beneath the satellites' orbits; thus for correcting single-frequency altimeter measurements.

For each DORIS mission one additional constant offset per 24 h is estimated in order to account for systematic effects. A model resolution of $J_\lambda = 2,\ J_\phi = 4,\ J_t = 3$ (L243) was used since the DORIS data provides relatively high spatial resolution along the satellites tracks (latitude direction) and sparse resolution in longitudinal direction. The measurement time interval of DORIS was reduced to about 1 min to avoid data correlations.

The validation of the model results is performed by comparison with Jason-2 altimeter VTEC measurements. For the complete time period of two months the differences between the model and the RA VTEC measurements were analyzed in order to get a good coverage of different local times for the VTEC measurements. Within 60 days, LTAN of Jason-2 orbit will vary by about 12 h (cf. Table 1) such that the LT of measurements will cover 24 h (cf. Fig. 3).

Figure 10 illustrates the model differences with respect to Jason-2 VTEC derived from dual-frequency radar altimetry measurements. The top plot shows the daily standard deviations (σ_{J2}) of the VTEC differences for both, the DORIS models and IGS GIM. These values range between 3.5 and 6.5 TECU (with one outlier). For some altimeter tracks significant offsets up to 2 TECU between Jason-2 VTEC and DORIS VTEC remains (not shown). The same holds for IGS GIMs.

The inclusion of DORIS measurements improves the consistency to Jason-2 measurements for almost all days as can be seen in the bottom plot of Fig. 10. The largest improve-

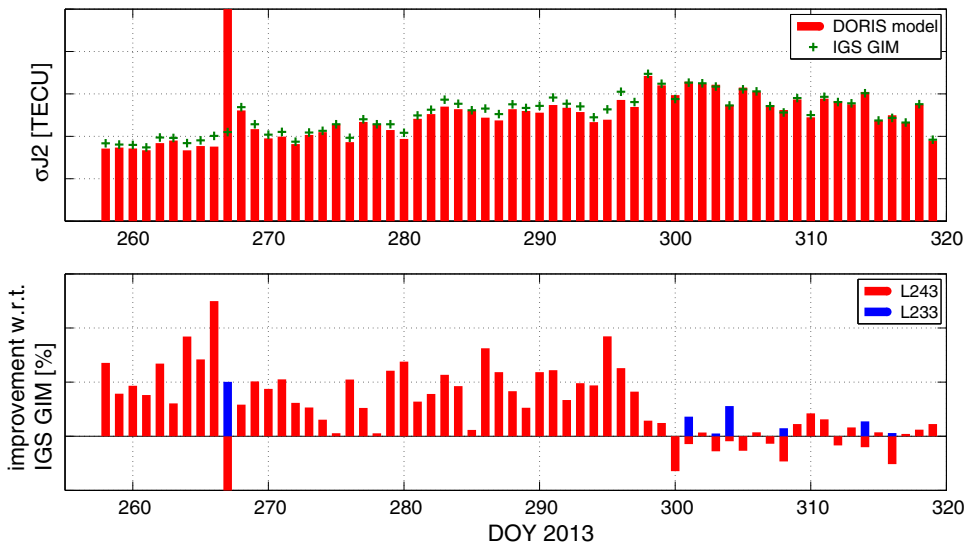

Fig. 10 Standard deviation σ_{J2} of the VTEC differences with respect to Jason-2 VTEC for the DORIS model (L243) and IGS GIM (*top plot*) and improvements when using DORIS-based models instead of pure IGS GIM (*bottom plot*). The *red bars* show the results for model resolution of L243; the *blue bars* indicate the results for L233 for some selected days

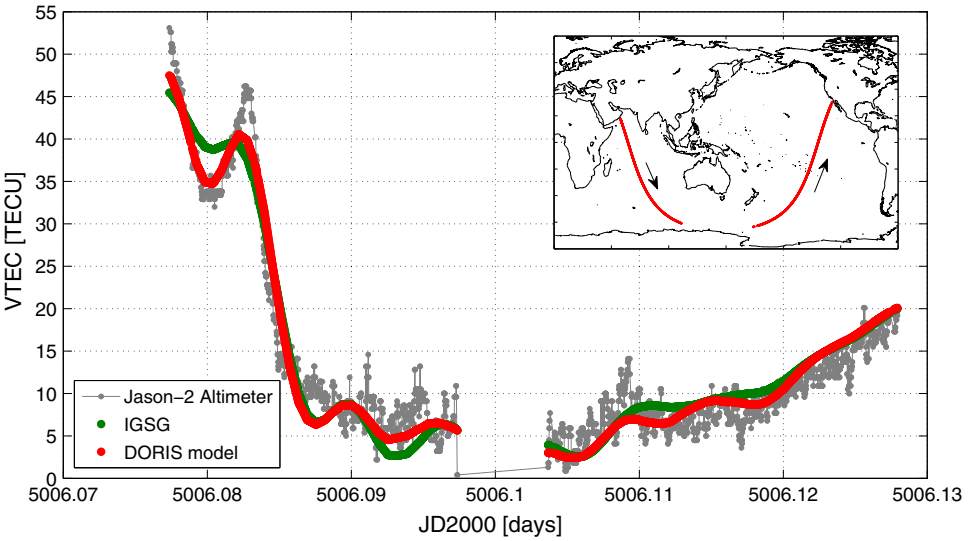

Fig. 11 VTEC on two Jason-2 altimeter passes (descending and ascending) on DOY258 from three different data sources: altimeter data is plotted in *gray*, IGS GIM in *green* and DORIS-based model (L243) in *red*

ment of σ_{J2} (0.5 TECU, 12 %) can be achieved for DOY266. For one day of the time period (DOY 267) the model resolution does not fit to the observations resulting as an outlier. By using a different model resolution of L233 one can reduce the σ_{J2} for this day from 28.4 to 4.0 TECU (IGS GIM achieves 4.2 TECU RMS). Changing the model resolution also improves the results for the last days of the time period. Thus, a fine-tuning of the model parameters or using a dedicated local model probably will further improve the results.

The reason for the small improvements towards the end of the time period is not fully understood. No correlation to the weighting between background model and DORIS data are detectable. It is also not possible to link this time period to local measurement times around noontime (highest solar radiation) for ascending or descending passes (cf. Fig. 3). However, there might be a connection to the increased solar activity after DOY297 (cf. Fig. 8, bottom plot). A relation to geomagnetic indices Kp and Ap is not visible. A more detailed investigation based on a longer time series would be helpful for fully understanding these connections.

For single passes, the improvements invoked by the integration of DORIS VTEC values turn out to be higher then anticipated from the mean standard deviations. This is illustrated in Fig. 11 where for two single altimeter profiles the VTEC data from different sources are plotted. In the first part of the profile (around Julian Day JD 5006.08, corresponding to DOY 258/2013, 13:55 UTC) one can identify an improvement of about 5 TECU coming from the inclusion of DORIS VTEC into the IGS GIM.

These results clearly show that DORIS can improve the IGS models significantly, at least in the region around the satellites' ground-tracks. The DORIS-supported models

show better consistency with altimetry for large time periods during medium solar activity.

Of course, not all of the remaining differences of about 3–6 TECU standard deviation are errors within the DORIS observations or the modeling. The altimeter noise has also an important influence. Although the Jason-2 VTEC is already smoothed (with a 20 s median filter) small scale variations are still visible (cf. Fig. 11). In order to get an impression on the amount of noise in the data a stricter filtering is performed for two test days. The standard deviation of the differences between the original Jason-2 VTEC and this super-smoothed version is about 2.5 TECU and the differences are visually normal distributed. Thus, one can conclude that the level of accuracy of the IGS GIMs with additional DORIS VTEC ranges between 1.5 and 3.5 TECU (1σ).

Although the absolute improvement by using DORIS in addition to IGS GIM is less than 1 TECU one should keep in mind that the model used in this study is a global one and not designed for local modeling. A more pronounced improvement can be expected when using dedicated local models beneath the satellites' ground-tracks.

5 Conclusion and outlook

The derivation of DORIS VTEC from dual-frequency phase observations is similar to the procedures applied for many years on terrestrial GNSS observations. However, some key differences have to be considered. The most challenging task is the estimation of the absolute level of VTEC as the DORIS pseudo-range observations can not be used for this purpose.

The derived DORIS VTEC observations show good consistency with external global models. Although the mean differences cannot be interpreted as they are arbitrarily forced to zero by using IGS GIMs the RMS of the differences can be analyzed: values around 2 TECU are achieved for the whole data set. When using only observations with elevation angles above 50° the RMS values of all missions keep well below 1 TECU for moderate solar conditions and do not exceed 2.1 TECU in the whole time period of investigation. All four DORIS missions analyzed (Jason-2, Cryosat-2, HY-2A, and SARAL) provides nearly the same level of accuracy. Only Cryosat-2 yields slightly worse performance than the other three missions.

Due to the orbit configuration of the DORIS missions the continuous computation of high-resolution DORIS-only global VTEC models is impossible today. However, the DORIS VTEC observations can be of great value for ionosphere modeling when combined with other space-geodetic input data such as terrestrial GNSS since they help to reach a more homogenous data distribution. Including DORIS into GPS derived VTEC models can improve the consistency with RA VTEC by more than 10 %.

When updating IGS GIM with DORIS VTEC the differences with respect to Jason-2 altimeter improve by up to 0.6 TECU using a global model approach. Probably, this can be further improved by adapting the model to the observation geometry, e.g. perform a local modeling just along the satellite's ground track. Thus, DORIS VTEC can help to improve ionospheric corrections for single-frequency altimeter systems as the measurements are taken on the same platform and should be optimal distributed for local modeling. This should be investigated in more detail within further studies.

Moreover, DORIS may add an important contribution to 4-dimensional (longitude, latitude, time, and height) ionosphere modeling as described e.g. in Limberger et al. (2013) since the DORIS STEC measurements can significantly improve the vertical geometry of the input observations when combined with other techniques such as terrestrial GNSS, RO, and altimetry.

Acknowledgments The authors gratefully acknowledge the following services and institutions for providing the input data for this study: IDS (DORIS data and satellites' orbits), IGS (GPS data, satellites' orbits and GIM), UCAR/CDAAC (COSMIC data), AVISO/NASA/CNES (Jason-2 data), and NOAA NGDC (F10.7 index). Moreover, we want to thank Remko Scharroo for providing the VTEC scaling factors.

References

Alizadeh M, Schuh H, Todorova S, Schmidt M (2011) Global ionosphere maps of VTEC from GNSS, satellite altimetry, and formosat-3/COSMIC data. J Geod 85(12):975–987. doi:10.1007/s00190-011-0449-z

Auriol A, Tourain C (2010) DORIS system: the new age. Adv Space Res 46(12):1484–1496. doi:10.1016/j.asr.2010.05.015

Bernhardt PA, Siefring CL (2010) Low-latitude ionospheric scintillations and total electron content obtained with the CITRIS instrument on STPSat1 using radio transmissions from DORIS ground beacons. Adv Space Res 45(12):1535–1540. doi:10.1016/j.asr.2009.12.001

Bilitza D, Reinisch B (2008) International Reference Ionosphere 2007: improvements and new parameters. Adv Space Res 42(4):599–609. doi:10.1016/j.asr.2007.07.048

Cerri L, Ferrage P (2014) DORIS satellites model implemented in POE processing, Ed.1, Rev. 6. SALP-NT-BORD-OP-16137-CN, CNES, ftp://ftp.ids-doris.org/pub/ids/satellites/DORISSatelliteModels

Dettmering D, Heinkelmann R, Schmidt M (2011a) Systematic differences between VTEC obtained by different space-geodetic techniques during CONT08. J Geod 85(7):443–451. doi:10.1007/s00190-011-0473-z

Dettmering D, Schmidt M, Heinkelmann R, Seitz M (2011b) Combination of different space-geodetic observations for regional ionosphere modeling. J Geod 85(12):989–998. doi:10.1007/s00190-010-0423-1

Dettmering D, Schmidt M, Limberger M (2013) Contributions of DORIS to ionosphere modeling. In: Ouwehand L (ed) Proceedings of "20 Years of Progress in Radar Altimetry", IDS Workshop, Sept. 2012, Venice, Italy, ESA Special Publication SP-710 (CD-Rom). doi:10.5270/esa.sp-710.altimetry2012

Dow J, Neilan R, Rizos C (2009) The international GNSS service in a changing landscape of global navigation satellite systems. J Geod 83(3–4):191–198. doi:10.1007/s00190-008-0300-3

Fleury R, Foucher F, Lassudrie-Duchesne P (1991) Global TEC measurement capabilities of the DORIS system. Adv Space Res 11(10):51–54. doi:10.1016/0273-1177(91)90321-A

Fong CJ, Yen NL, Chu CH, Yang SK, Shiau WT, Huang CY, Chi S, Chen SS, Liou YA, Kuo YH (2009) FORMOSAT-3/COSMIC spacecraft constellation system, mission results, and prospect for follow-on mission. Terr Atmos Ocean Sci 20:1–19. doi:10.3319/TAO.2008.01.03.01(F3C)

Foucher F, Ciavaldini JF (1991) Modeling the ionospheric electron content for the correction of altimetric measurements. Pure Appl Geophys 135(3):475–491. doi:10.1007/BF00879476

Hernández-Pajares M, Juan JM, Sanz J, Orus R, Garcia-Rigo A, Feltens J, Komjathy A, Schaer SC, Krankowski A (2009) The IGS VTEC maps: a reliable source of ionospheric information since 1998. J Geod 83(3–4):263–275. doi:10.1007/s00190-008-0266-1

Hilla S (2010) The extended standard product 3 orbit format (SP3-c). http://igscb.jpl.nasa.gov/igscb/data/format/sp3c.txt

Hugentobler U, Schaer S, Beutler G, Bock H, Dach R, Jäggi A, Meindl M, Urschl C, Mervart L, Rothacher M, Wild U, Wiget A, Brockmann E, Ineichen D, Weber G, Habrich H, Boucher C (2002) CODE IGS analysis center technical report 2002. Tech. rep., IGS 2001 / 2002 Technical Reports

IDS (2012) Modelling of DORIS instruments, Version 16.2. ftp://ftp.ids-doris.org/pub/ids/satellites/DORIS_instrument_modelling_1G_envisat

Iijilma B, Harris I, Ho C, Lindqwister U, Mannucci A, Pi X, Reyes M, Sparks L, Wilson B (1999) Automated daily process for global ionospheric total electron content maps and satellite ocean ionospheric calibration based on global positioning system. J Atmos Solar Terr Phys 61(16):1205–1218. doi:10.1016/S1364-6826(99)00067-X

Koch K, Kusche J (2002) Regularization of geopotential determination from satellite data by variance components. J Geod 76(5):259–268. doi:10.1007/s00190-002-0245-x

Li F, Parrot M (2007) Study of the TEC data obtained from the DORIS stations in relation to seismic activity. Ann Geophys 50(1):39–50. doi:10.4401/ag-3086

Limberger M, Liang W, Schmidt M, Dettmering D, Hugentobler U (2013) Regional representation of F2 Chapman parameters based on electron density profiles. Ann Geophys 31(12):2215–2227. doi:10.5194/angeo-31-2215-2013

Lourme E (2010) RINEX DORIS 3.0. SALP-SP-M-EA-15578-CN, Issue 1.3, CNES. ftp://ftp.ids-doris.org/pub/ids/data/RINEX_DORIS

Mercier F, Cerri L (2010) DORIS phase mesurements and ionospheric effects. Presentation given at the IDS Workshop 2010, Lisbon. http://ids-doris.org/images/documents/report/ids_workshop_2010/IDS10_s4_Mercier_PhaseMeasurementsIonoEffects

Mercier F, Cerri L, Berthias JP (2010) Jason-2 DORIS phase measurement processing. Adv Space Res 45(12):1441–1454. doi:10.1016/j.asr.2009.12.002

NOAA (2014) F10.7 index. ftp://ftp.ngdc.noaa.gov/STP/GEOMAGNETIC_DATA/INDICES/KP_AP/

Petit G, Luzum B (2010) IERS conventions (2010), IERS technical note 36. Verlag des Bundesamts für Kartographie und Geodäsie, Frankfurt am Main

Scharroo R, Smith W (2010) A global positioning systembased climatology for the total electron content in the ionosphere. J Geophys Res 115(A10318):16. doi:10.1029/2009JA014719

Schmidt M, Dettmering D, Mößmer M, Wang Y, Zhang J (2011) Comparison of spherical harmonic and B spline models for the vertical total electron content. Radio Sci 46(6). doi:10.1029/2010RS004609

Schueler T (1998) On the interpolation of SP3 orbit files. Tech. rep., Institute of Geodesy and Navigation, University FAF Munich, IFEN-TropAC-TN-002-01

Schumaker L, Traas C (1991) Fitting scattered data on spherelike surfaces using tensor products of trigonometric and polynomial splines. Numer Math 60(1):133–144. doi:10.1007/BF01385718

Todorova S, Schuh H, Hobiger T, Hernández-Parajes M (2007) Global models of the ionosphere obtained by integration of GNSS and satellite altimetry data. Österreichische Zeitschrift für Vermessung und Geoinformation (VGI) 2:80–89

Willis P, Soudarin L, Jayles C, Rolland L (2007) DORIS applications for solid Earth and atmospheric sciences. Compt Rendus Geosci 339(16):949–959. doi:10.1016/j.crte.2007.09.015

Willis P, Fagard H, Ferrage P, Lemoine FG, Noll CE, Noomen R, Otten M, Ries JC, Rothacher M, Soudarin L, Tavernier G, Valette JJ (2010) The international DORIS service toward maturity. Adv Space Res 45(12):1408–1420. doi:10.1016/j.asr.2009.11.018